Observations and analysis of an urban boundary layer during extreme heat events

Gabriel Rios [1*, 2*], Prathap Ramamurthy [1, 2]

1. Department of Mechanical Engineering, CUNY City College, New York, New York
2. NOAA Center for Earth System Sciences and Remote Sensing Technologies, New York, New York

Corresponding author: Gabriel Rios (grios001@citymail.cuny.edu)

*** Current affiliation(s)**: Department of Mechanical Engineering, CUNY City College, New York, New York; NOAA Center for Earth System Sciences and Remote Sensing Technologies, New York, New York

For submission to the Quarterly Journal of the Royal Meteorological Society.
Last updated: February 14, 2022.

Abstract

Extreme heat presents a significant risk to human health and infrastructure in cities. Several studies have been conducted in the past two decades to understand the interaction between the synoptic-scale extreme heat events and local-scale urban heat island effects. However, observations of boundary layer characteristics during these periods have been relatively rare. Our current understanding of boundary layer dynamics is incomplete, particularly in coastal urban environments where the local climatology is highly influenced by land-sea thermal gradients. Here we analyze the evolution and structure of the urban boundary layer during regular and extreme heat periods. Our primary goal is to understand how boundary layer dynamics during extreme heat events regulate near-surface transport of mass, momentum, and heat. The analysis will also focus on how the urban surface layer interacts with the mixed layer during these events. Our analysis focuses on the New York City metropolitan area and relies on observations from vertical profilers (Doppler lidar, microwave radiometer) and quantities derived by analytical methods. Additionally, satellite and reanalysis data are used to supplement observational data.

1 Introduction

Extreme heat poses a major risk to life and property. The effects of extreme heat are expected to impact cities especially, which presents a significant hazard for vulnerable populations and infrastructure. With regards to effects on public health, studies have shown that extreme and prolonged heat increases mortality and exacerbates existing health conditions in high-risk populations (Anderson and Bell, 2011; Frumkin, 2016; Heaviside, Macintyre, and Vardoulakis, 2017; Madrigano et al., 2015). With regards to effects on infrastructure, studies have shown that extreme heat subjects networks critical to urban areas (e.g., electrical grid, public transportation) under significant stresses and/or failure (McEvoy, Ahmed, and Mullett, 2012; Zuo et al., 2015). These events are projected to increase in frequency due to the effects of climate change. Projections indicate that the impacts of future climate will cause adverse effects of extreme heat to become more frequent and severe (Burillo et al., 2019; Forzieri et al., 2018; Peng et al., 2011).

The meteorology of extreme heat events and its impacts on urban areas can be observed from the synoptic and local scales. From a synoptic scale, extreme heat events are often caused by the sustained presence of a high-pressure system over an area, resulting in lower wind speeds and warm air subsidence, promoting higher surface temperatures (Black et al., 2004; Miralles et al., 2014). From a local perspective, the amplified impact of extreme heat events on cities is a result of the urban heat island (UHI) effect, which occurs as a result of the modification of land surface properties due to the built environment. The modification of surface properties has been shown to increase near-surface air temperatures due to factors such as radiation entrapment, increased heat storage, and lower evapotranspirative cooling (Chen, Yang, and Zhu, 2014; Li and Elie Bou-Zeid, 2013; Ramamurthy and Bou-Zeid, 2017; Zhao et al., 2018). Additionally, urban areas near large bodies of water experience effects from the sea breeze, which has been shown to play a moderating influence on the intensity of the UHI effect (Hu and Xue, 2016; Jiang et al., 2019; Stéfanon et al., 2014). The processes on these two scales can be connected by understanding the structure and dynamics of the urban boundary layer (UBL), which is the lowest part of the troposphere in which surface-atmosphere exchanges occur that directly affect human activity. There have been a large number of numerical studies performed to improve our understanding of UBL processes during extreme heat events, which have been important for conceptualizing the role of synoptic-scale and surface forcings on urban climate. Something about the vertical structure of the UBL and coupling these

However, detailed observational analyses of UBL structure and dynamics are somewhat limited, especially in the vertical direction. Over the last 20 years, microwave radiometers, lidars, and radiosondes have been shown to be essential for accomplishing this. Microwave radiometers have been used to determine vertical profiles of temperature and water vapor (Rose et al., 2005; Z. Wang et al., 2012), while lidars being used to observe three-dimensional wind fields and aerosol concentrations (Grund et al., 2001). Although radiosondes provide direct measurements of the aforementioned properties in the boundary layer as it moves vertically through it, they present greater difficulties (e.g., cost, shorter supply) and are unable to observe at the temporal resolution of microwave radiometers and lidars.

Although somewhat limited in spatiotemporal scale, numerous observational campaigns have been performed to better our understanding of UBL structure and dynamics. Barlow et al. (2011) provides an in-depth study of boundary layer dynamics above London over a month-long period using a combination of a sonic anemometer and Doppler lidar, allowing for high-resolution vertical observations of a complex UBL and a better understanding of turbulent structures and vertical mixing processes. Similarly, Pelliccioni et al. (2012) employs a sonic anemometer and a sodar system at a site in Rome to observe and analyze the lower 200 m of the UBL to determine UBL characteristics and explore the validity of Monin-Obukhov similarity theory in the surface layer. Additionally, Arruda Moreira et al. (2020) evaluates the ability of lidar and microwave radiometer systems to observe turbulence over a variety of atmospheric conditions, including the effects of significant dust concentrations, in the region around Granada, Spain. Studies such as those performed by Banks et al. (2015), Quan et al. (2013), and Z. Wang et al. (2012) further demonstrate the ability of vertical profiling instruments to analyze the boundary layer structure by deriving UBL heights and its diurnal evolution. Expanding upon UBL structure, Anurose, Subrahamanyam, and Sunilkumar (2018) details a long-term observational campaign over an urban location in southern India that chronicles UBL height through monsoon season, annual averages of near-surface quantities, and the dynamics and effects of the sea breeze circulation.

Observations of the UBL during extreme heat events are even more limited. Ramamurthy and Bou-Zeid (2017) used microwave radiometers to observe the UBL over New York City in July 2016 to find that the UHI effect was amplified during heat wave events and that spatial variability throughout the city was significant throughout the observation period. Jiang et al. (2019) explores the effects of heat waves on rural and urban areas for several cities in China using ground-based observations with a focus on the UHI effect, finding that the effect was amplified during heat waves due to greater surface solar radiation and shifts in wind direction contributing to advection of heated air masses over the studied cities. (Wu et al., 2019) uses a combination of a ceilometer and multiple lidars to observe the evolution of UBL structure, air quality, and pollutant transport during a heat wave in New York City, demonstrating sharp rates of UBL growth due to convective activity and an increase of pollutant concentration and regional transport.

Zhang et al. (2020) uses aircraft-based observations to provide a comprehensive analysis of UBL structure during heat wave events over cities in the United States throughout a 10-year period, providing insights into the 'heat dome' thermodynamic structure over cities and the variability between heat wave events due to local (such as surface properties in urban areas) and large-scale (such as synoptic meteorological conditions) forcings.

New York City represents a complex case for urban meteorology given its diverse array of land cover types (deciduous forest to supertall skyscrapers) and its proximity to multiple major bodies of water (Lower New York Bay and the New York Bight to the south and east, Long Island Sound to the north and east). Due to these factors, the effects of the surface energy budget (Hrisko, Prathap Ramamurthy, and Gonzalez, 2021; Prathap Ramamurthy and Bou-Zeid, 2014; Tewari et al., 2019) and sea breezes (Childs and Raman, 2005; Colle and Novak, 2010; Frizzola and Fisher, 1963; Gedzelman et al., 2003; Melecio-Vázquez et al., 2018; Thompson, Holt, and Pullen, 2007) on the mesoscale meteorology have been studied extensively. However, similar to studies of other urban areas mentioned previously, much of this research has involved numerical simulations of these meteorological processes. In this study, we attempt to further our understanding of the UBL over a coastal urban area by compiling observations from multiple locations within New York City and analyzing the UBL using derived quantities.

This study attempts to use observations and analytical methods to provide insight into the following questions:

1. How do UBL structure and dynamics depart from the climatology during extreme heat events?
2. How does the UBL structure impact the transport of scalars?
3. What effect does the sea breeze have on a coastal urban area during extreme heat events?

2 Data collection and analysis

2.1 Study site

The UBL over New York City is observed and analyzed in this study. Observational data was captured at four locations within New York City (Table 1).

Table 1: Locations and details of observations sites.

	Bronx	Queens	Staten Island
Coordinates	40.87248°N, -73.89352°E	40.73433°N, -73.81585°E	40.60401°N, -74.14850°E
Elevation (m a.g.l.)	57.8	56.3	32.4
Element roughness height (m a.g.l.)			
Valid wind directions	N/A	180 to 360°	N/A

2.2 Observational instruments

Observations of the UBL were made using a synthesis of microwave radiometers, lidars, and satellites.

Vertical profiles of temperature and vapor density were captured using a network of Radiometrics MP-3000A microwave radiometers (Hewison and Gaffard, 2003) operated by the New York State Mesonet (Brotzge et al., 2020). Profiles for water vapor are retrieved using 21 channels in the 22-30.0 GHz (K-band) range, while profiles for temperature are retrieved using 14 channels in the 51-59.0 GHz (V-band) range. Profile accuracy (relative to radiosonde soundings) determined by performance studies at various locations reported an annually-averaged water vapor accuracy within $1.0\,\mathrm{g\,m^{-3}}$ below $2\,\mathrm{km}$

and an annually-averaged temperature accuracy within 1.6 K below 4 km (Güldner and Spänkuch, 2001; Sánchez et al., 2013). Quantities are captured at 58 height levels starting at ground level and ending at 10 km above ground level, with vertical steps of 50 m from ground level to 500 m, 100 m from 500 m to 2 km, and 250 m steps above 2 km. Observation integration times range from 0.01 to 2.50 s. Vertical profiles are generated every 10 s and averaged over 10 min periods.

Wind measurements were measured using a network of Leosphere WindCube 100S Doppler lidars operated by the New York State Mesonet (Brotzge et al., 2020). Measurements of wind motion using the Doppler beam swinging scan mode in three directions: zonal (u), meridional (v), and vertical (w) over 20 s cycles, with measurements averaged over 10 min intervals (Shrestha et al., 2021). The vertical range of the WindCube 100S is 7 km above ground level with wind speed and direction accuracies of $0.5\,\mathrm{m\,s^{-1}}$ and 2°, respectively. The WindCube 100S has also been shown to perform with a high degree of accuracy relative to radiosonde soundings, especially above 500 m (Kumer, Reuder, and Furevik, 2014).

Land and sea surface temperatures were estimated using derived products from the NOAA/NASA GOES-16 Advanced Baseline Imager (ABI) (Ignatov et al., 2010; Yu et al., 2008). The GOES-16 ABI provides a spatial resolution of 2 km with real-time data available to the public on an hourly basis. The spatial extent of the Land Surface Temperature (LST) product ranges from the continental United States (CONUS) to the majority of the Western Hemisphere (known as *full disk*), whereas the Sea Surface Temperature (SST) product has a full disk spatial extent. The LST product has been found to have an error relative to surface observations of 2.5 K over all land cover types, while sea surface temperatures (SSTs) estimated using the GOES-16 ABI have been found to have an error relative to shipborne radiometers ≤ 1 K in the New York Bight (Luo and Minnett, 2021).

2.2.1 Data criteria & availability

Dates selected for this study are categorized into three groups: (1) normal days, (2) extreme heat days, and (3) sea breeze days. For the purposes of this study, *extreme heat events* are defined as 3 or more consecutive days with maximum daily temperatures exceeding 90°F (305 K), per the New York branch of NOAA National Weather Service (Robinson, 2001; National Weather Service, 2018), while *normal days* are defined as days that do not meet these criteria. Because the aim of this study is to observe the effect of extreme heat on the UBL, normal day selection was restricted to months in which extreme heat events occurred (May through September), as well as days in which 50% or more of the day featured clear-sky conditions below 3.65 km above ground level due to the association of extreme heat events with reduced daytime cloud coverage and precipitation (Stéfanon et al., 2014; Thomas et al., 2020). Clear-sky conditions were identified by using an average of 5-minute surface-based observations from three airports in the Automated Surface Observation System (ASOS) (NOAA et al., 1998) network within the New York City metropolitan area: Newark Liberty International Airport (EWR), John F. Kennedy International Airport, and LaGuardia Airport. *Sea breeze events* are identified as times during normal and extreme heat days in which the low-level (≤ 200 m) mean horizontal wind speed (U) is less than $5\,\mathrm{m\,s^{-1}}$ and low-level wind direction has a primarily easterly component, due to the presence of the Atlantic Ocean to the east of New York City.
- Discuss quality filtering - Plots showing sampling counts per hour per site per day

2.3 Derived quantities

3 Normal and extreme heat boundary layer properties

This section discusses the differences in boundary layer structure and properties between normal days and extreme heat events. Results are presented from the averages over all identified normal and heat event days.

3.1 Temperature

On average, extreme heat events increase the temperature at the surface, as expected (see Figure 4). This is consistent across all observed locations in New York City, with the extreme heat event temperature exceeding normal temperatures by approximately 1-σ over the entire day. An increase in the difference is observed during daytime hours, with the difference peaking in magnitude around 13:00 LST at the hottest time of day. The surface temperature variability is significantly lower during heat events ($\sigma = 1.77\,\mathrm{K}$) than during normal temperatures ($\sigma = 4.57\,\mathrm{K}$).

Above the surface, extreme heat events similarly increase the temperature significantly over the lowest 3000 m of the troposphere (see Figure 3), with standardized anomalies of θ ranging from $\sigma = 0.88$ to 1.20. The largest temperature anomalies shift from the surface layer in the mornings to span the entirety of the mixed layer. This is reflective of strong surface forcing resulting in convection through the surface layer, as indicated by the formation of a late morning superadiabatic layer at all locations (Figures 5, 6, 7).

The vertical profiles of θ suggests a degree of spatial variability exists between locations. One instance of this spatial variability is vertical mixing; the Bronx site appears to have stronger vertical mixing based on Figure 5, as θ remains constant for a greater height than at the Queens and Staten Island locations. This phenomenon is more pronounced during extreme heat events, as a distinct mixed layer is apparent in the Bronx during early (12:00 LST) and late (18:00 LST) afternoon hours. While the mixed layer is also visible for the other locations, the strength of the mixed layer is emphasized by the negative $\frac{d\theta}{dz}$ values between 1000 and 1500 m.

3.2 Moisture

On average, extreme heat events were found to increase the moisture at the surface, as indicated by the diurnal profiles of specific humidity (q) (see Figure 9). This is also consistent across all observed locations in New York City, with the extreme heat event temperature exceeding normal temperatures by approximately 1-σ over the entire day. Although a distinct diurnal profiles exists (q decreases during daytime hours), the diurnal range is smaller in magnitude than temperature. It is also worth noting that the diurnal range is lower for Staten Island than for the Bronx or Queens, suggesting that degree of urbanization has a negative correlation with the diurnal range of q. Similar to surface temperature, the variability of q is significantly lower during heat events ($\sigma = 2.14 \times 10^{-3}\,\mathrm{kg\,kg^{-1}}$) than during normal temperatures ($\sigma = 3.18 \times 10^{-3}\,\mathrm{kg\,kg^{-1}}$).

In the boundary layer, the positive q anomalies subside in magnitude between 300 and 600 m, but increase significantly in the mixed layer, especially during the late morning and early afternoon for all sites. As shown in Figure 8, the largest anomalies occur between 10:00 and 16:00 LST in the upper mixed layer. With regards to spatial variation in q, the highest anomalies occur over the Bronx and Queens, whereas Staten Island demonstrates a positive q anomaly with lower magnitudes during extreme heat events. This correlates with the magnitude of the difference in surface quantities shown in Figure 9.

With regards to time, mid-morning increases in anomaly values in the lower mixed layer ($\sim$500 m) suggest enhanced vertical transport of moisture across all sites (see Figures 10, 11, 12). Vertical profiles of q across all locations show markedly higher q values at the surface during extreme heat event with $\frac{dq}{dz}$ values increasing throughout the morning in the mixed layer while low-level q values decrease, indicating vertical transport of moisture and drier low-level conditions during peak insolation.

3.3 UBL dynamics

3.3.1 Horizontal winds

Extreme heat events coincided with an overall reduction of horizontal wind speeds (U) in the UBL. More specifically, the magnitude of U during extreme heat events is similar in magnitude to U during normal days with the exception of early morning hours and at upper levels of the UBL. As shown in Figure 13, modest reductions in U ($-1.2 \leq \sigma \leq -0.4$) during extreme heat events are present throughout the UBL from early to mid-morning, with little differences throughout the rest of the day ($-0.4 \leq \sigma \leq 0.4$). Larger deviations between U values are present at the top of the UBL where synoptic conditions become dominant.

Vertical profiles of U for normal and extreme heat events provide a more detailed view of the differences in UBL structure. Across all sites, U is similar throughout the UBL overnight, afternoon, and evenings. During early morning hours, extreme heat event U values decrease by 25 to 50% throughout the entire UBL (see Figures 15, 16, 17), although both event types present a classical logarithmic wind profile, with surface friction effects present through 500 m. Another phenomenon worth noting is the difference in U profiles above 2000 m; profiles of U during extreme heat events are more consistent between sites and vertically than during normal days. This phenomenon may highlight the effect of synoptic meteorological conditions on U, as the UBL typically remains below 2500 m. During extreme heat events, anticyclonic conditions produce more stable atmospheric conditions relative to normal days, resulting in less variability between heat events than during normal days.

Extreme heat events result in a southwesterly shift in U throughout the UBL. This shift is present most evidently closer to the surface, as shown in Figures 18, 19, and 20, with winds at 100 m coming primarily from the southwest quadrant. Figure 19 shows that Queens also presents a secondary maximum with winds approaching from the south, which suggests effects from the Atlantic sea breeze (effects from the sea breeze will be further discussed in Section 4). At 1000 m, the directionality of prevailing winds becomes more uniform between normal and extreme heat days, as winds primarily approach New York City from the west-southwest. The disparity in wind directions between 100 and 1000 m suggests that localized wind fields play a major role in UBL dynamics at lower levels whereas synoptic-scale atmospheric conditions increasingly dominate with increasing height.

3.3.2 Vertical motion

On average, extreme heat events do not appear to produce significant changes in vertical velocity (w). Figure 21 shows average diurnal profiles of w at all locations at 100 m above ground level, with similar mean values throughout the day between normal days and extreme heat events. During extreme heat events, however, the variability of w is less in the early morning hours and greater in the evening. This phenomenon is also observed in vertical profiles of w at all locations as shown in Figures 23,24, and 25. At all locations, overnight and morning profiles of w (0:00 and 6:00 LST) show significantly lower variability in w throughout the UBL with similar magnitudes of mean w. Despite similar means and deviations in the early afternoon (12:00 LST), evening profiles (18:00 LST) show significantly higher variability in w below 500 m for all sites, with the Bronx showing this occurrence extend through the UBL.

4 Effects of the sea breeze circulation

Sea breezes in New York City occur as a result of land-sea temperature gradients from two arms of the Atlantic Ocean; the New York Bight to the southeast and Long Island Sound to the northeast. Sea breezes from both bodies increase the complexity of UBL dynamics over New York City due to the coalescence of opposing fronts over a complex topography (Bornstein and Thompson, 1981). A typical sea breeze event in New York City is defined by calm ambient low-level winds ($\leq 5\,\mathrm{m\,s^{-1}}$, the formation of a large land-sea temperature gradient in the mid- to late morning, strong late-morning thermals that promote low-level convergence, and afternoon to early-evening onshore moisture transport and reduction in surface air temperatures (especially in areas closest to the shore) (Childs and Raman, 2005; Frizzola and Fisher, 1963; Gedzelman et al., 2003).

Sea breeze events occurred on approximately 56% of all days observed. The high frequency of occurrence is likely attributable to the large land-sea temperature gradient that is common during warmer months (Gedzelman et al., 2003), as days were chosen exclusively between May and September. Maximum land-sea surface temperature differences during days with identifiable sea breeze events averaged at 12 K, with a strong diurnal profile with the peak difference occurring around midday (see Figure 26). The frequency of occurrence increases when observing days during extreme heat events, as the lack of a strong synoptic wind allows for the sea breeze circulation to become dominant in the metropolitan area (Miller et al., 2003).

4.1 UBL structure during sea breeze events

During normal days, observations show that the sea breeze reduces temperatures and increases moisture content throughout the UBL after 12:00 LST. In Figure 27, the standardized anomalies of θ between normal days with and without a sea breeze are shown, averaged over all days for each set of days. Overnight and in the early morning, positive anomalies of θ are present above the UBL ($\leq 1\,\mathrm{km}$) until mid-morning, with the Bronx having the most significant anomaly and Staten Island the least. This suggests a decreasing degree of anomalous θ with decreasing urbanization. This anomaly pattern coincides with a positive q anomaly trend in both the spatiotemporal aspect (peak anomaly occurs above 1 km before 8:00 LST) and the magnitude aspect (the Bronx has the most significant early morning anomaly, Staten Island has the least). Later in the day, all sites observe a negative θ anomaly throughout the UBL despite a negative q anomaly, indicating that sea breeze events during normal days coincide with a cooler and drier daytime UBL. Sea breeze effects become apparent during the mid-afternoon with the presence of a significant negative θ and positive q anomaly in the lower UBL, with Staten Island experiencing effects first (approximately 16:00 LST) and the Bronx experiencing effects last. It is worth noting that the q anomaly is weakest in the Bronx, indicating that the sea breeze front weakens as it travels inland over New York City.

During extreme heat events, observations show that the sea breeze plays a moderating role on surface conditions by reducing low-level temperatures and increasing low-level moisture content, similar to phenomena observed during normal days. In Figure 29, the standardized anomalies of θ between extreme heat days with and without a sea breeze are shown, averaged over all days. All sites shown that extreme heat days with a sea breeze possess slightly higher values of θ in the mid-morning, with significant low-level reduction in θ in the afternoon and evening. On average, the onset of the low-level cooling occurs in Staten Island first at approximately 12:00 LST, with Queens following at approximately 14:00 LST, and the Bronx at about 18:00 LST. This disparity in times appears to represent the passage of the southeasterly sea breeze front through New York City, where the onset time correlates with the distance from the New York Bight (Bornstein and Thompson, 1981). A similar phenomenon is observed by the transport of q as shown in Figure 30, with drier conditions throughout the UBL before 12:00 LST and increasing low-level moisture as the day progresses. With regards to onset, q follows a similar pattern to θ in that the onset time is dependent from distance to the shore.

These anomalies present most significantly in the lowest 1000 m of the UBL after 12:00 LST, which aligns with sea breeze circulation characteristics observed in Frizzola and Fisher (1963).

4.2 UBL dynamics during sea breeze events

Days with identifiable sea breeze events had lower U throughout the majority of the UBL, with the most significant decreases during the nighttime, potentially due to the lessening of onshore flow due to the reduction of the land-sea temperature gradient (Pullen et al., 2007), as shown in Figure 26. Vertical motions, however, increased significantly in the Bronx and Queens during the late morning and early afternoon, as shown in Figure 31. These anomalies likely indicate the increased presence of updrafts in urbanized areas.

During days with identified sea breeze circulations, easterly winds increase in frequency in the lower levels of the UBL, as shown in Figures 32, 33, and 34. Southeasterly winds (due to sea breezes from the New York Bight) increased in frequency compared to all other days at all locations. The occurrence frequency of southeasterly winds is correlated with the distance between the observation site and the largest body of water in proximity of the metropolitan area (Atlantic Ocean), as Staten Island reported 92.1% of all winds at 100 m as southeasterly between 12:00 and 20:00 LST (distance of 6.50 km from Lower New York Bay), whereas Queens reported 67.4% (distance of 16.5 km), and Bronx reported 55.6% (distance of 32.9 km).

For sites near Long Island Sound (the Bronx and Queens), northeasterly winds increased in frequency as well, though not to the same magnitude as southeasterly winds. This disparity in magnitude suggests that the Long Island Sound sea breeze front is weaker than the New York Bight sea breeze front, which aligns with previous studies of sea breeze fronts over New York City (Frizzola and Fisher, 1963; Meir et al., 2013).

5 Conclusions

- How do UBL structure and dynamics depart from the climatology during extreme heat events?
- How does the UBL structure impact the transport of scalars?
- The sea breeze reduces temperatures throughout the UBL after the onset of the sea breeze, which typically occurs in the mid-afternoon in immediate coastal areas and in the evening for areas further inland. The sea breeze also results in nocturnal low-level onshore moisture transport.

Acknowledgments

This research is made possible by the New York State (NYS) Mesonet. Original funding for the NYS Mesonet was provided by Federal Emergency Management Agency grant FEMA-4085-DR-NY, with the continued support of the NYS Division of Homeland Security & Emergency Services; the state of New York; the Research Foundation for the State University of New York (SUNY); the University at Albany, SUNY; the Atmospheric Sciences Research Center (ASRC) at SUNY Albany; and the Department of Atmospheric and Environmental Sciences (DAES) at SUNY Albany.

References

Anderson, G Brooke and Michelle L Bell (2011). "Heat waves in the United States: mortality risk during heat waves and effect modification by heat wave characteristics in 43 US communities". In: *Environmental health perspectives* 119.2, pp. 210–218.

Anurose, TJ, D Bala Subrahamanyam, and SV Sunilkumar (2018). "Two years observations on the diurnal evolution of coastal atmospheric boundary layer features over Thiruvananthapuram (8.5° N, 76.9° E), India". In: *Theoretical and applied climatology* 131.1, pp. 77–90.

Arruda Moreira, Gregori de et al. (2020). "Study of the planetary boundary layer height in an urban environment using a combination of microwave radiometer and ceilometer". In: *Atmospheric Research* 240, p. 104932.

Banks, Robert F et al. (2015). "Performance evaluation of the boundary-layer height from lidar and the Weather Research and Forecasting model at an urban coastal site in the north-east Iberian Peninsula". In: *Boundary-layer meteorology* 157.2, pp. 265–292.

Barlow, Janet F et al. (2011). "Boundary layer dynamics over London, UK, as observed using Doppler lidar during REPARTEE-II". In: *Atmospheric Chemistry and Physics* 11.5, pp. 2111–2125.

Black, Emily et al. (2004). "Factors contributing to the summer 2003 European heatwave". In: *Weather* 59.8, pp. 217–223.

Bornstein, Robert D and William T Thompson (1981). "Effects of frictionally retarded sea breeze and synoptic frontal passages on sulfur dioxide concentrations in New York City". In: *Journal of Applied Meteorology and Climatology* 20.8, pp. 843–858.

Brotzge, Jerald A et al. (2020). "A technical overview of the new york state mesonet standard network". In: *Journal of Atmospheric and Oceanic Technology* 37.10, pp. 1827–1845.

Burillo, Daniel et al. (2019). "Electricity infrastructure vulnerabilities due to long-term growth and extreme heat from climate change in Los Angeles County". In: *Energy Policy* 128, pp. 943–953.

Chen, Feng, Xuchao Yang, and Weiping Zhu (2014). "WRF simulations of urban heat island under hot-weather synoptic conditions: The case study of Hangzhou City, China". In: *Atmospheric research* 138, pp. 364–377.

Childs, Peter P and Sethu Raman (2005). "Observations and numerical simulations of urban heat island and sea breeze circulations over New York City". In: *Pure and Applied Geophysics* 162.10, pp. 1955–1980.

Colle, Brian A and David R Novak (2010). "The New York Bight jet: climatology and dynamical evolution". In: *Monthly Weather Review* 138.6, pp. 2385–2404.

Forzieri, Giovanni et al. (2018). "Escalating impacts of climate extremes on critical infrastructures in Europe". In: *Global environmental change* 48, pp. 97–107.

Frizzola, John A and Edwin L Fisher (1963). "A series of sea breeze observations in the New York City area". In: *Journal of Applied Meteorology and Climatology* 2.6, pp. 722–739.

Frumkin, Howard (2016). "Urban sprawl and public health". In: *Public health reports.*

Gedzelman, SD et al. (2003). "Mesoscale aspects of the urban heat island around New York City". In: *Theoretical and applied climatology* 75.1, pp. 29–42.

Grund, Christian J et al. (2001). "High-resolution Doppler lidar for boundary layer and cloud research". In: *Journal of Atmospheric and Oceanic Technology* 18.3, pp. 376–393.

Güldner, J and D Spänkuch (2001). "Remote sensing of the thermodynamic state of the atmospheric boundary layer by ground-based microwave radiometry". In: *Journal of Atmospheric and Oceanic Technology* 18.6, pp. 925–933.

Heaviside, Clare, Helen Macintyre, and Sotiris Vardoulakis (2017). "The urban heat island: implications for health in a changing environment". In: *Current environmental health reports* 4.3, pp. 296–305.

Hewison, Tim and Catherine Gaffard (2003). "Radiometrics MP3000 microwave radiometer performance assessment". In: *Obs. Development Technical Report TR29, Met Office, National Meteorological Library, Exeter, UK. Also available from http://tim. hewison. org/TR29. pdf.*

Hrisko, Joshua, Prathap Ramamurthy, and Jorge E Gonzalez (2021). "Estimating heat storage in urban areas using multispectral satellite data and machine learning". In: *Remote Sensing of Environment* 252, p. 112125.

Hu, Xiao-Ming and Ming Xue (2016). "Influence of synoptic sea-breeze fronts on the urban heat island intensity in Dallas–Fort Worth, Texas". In: *Monthly Weather Review* 144.4, pp. 1487–1507.

Ignatov, A et al. (2010). "GOES-R Advanced Baseline Imager (ABI) algorithm theoretical basis document for sea surface temperature". In: *NOAA NESDIS Center for Satellite Applications and Research.*

Jiang, Shaojing et al. (2019). "Amplified urban heat islands during heat wave periods". In: *Journal of Geophysical Research: Atmospheres* 124.14, pp. 7797–7812.

Kumer, Valerie-M, Joachim Reuder, and Birgitte R Furevik (2014). "A comparison of LiDAR and radiosonde wind measurements". In: *Energy Procedia* 53, pp. 214–220.

Li, Dan and Elie Bou-Zeid (2013). "Synergistic interactions between urban heat islands and heat waves: The impact in cities is larger than the sum of its parts". In: *Journal of Applied Meteorology and Climatology* 52.9, pp. 2051–2064.

Luo, Bingkun and Peter J Minnett (2021). "Skin Sea Surface Temperatures From the GOES-16 ABI Validated With Those of the Shipborne M-AERI". In: *IEEE Transactions on Geoscience and Remote Sensing* 59.12, pp. 9902–9913.
Madrigano, Jaime et al. (2015). "A case-only study of vulnerability to heat wave–related mortality in New York City (2000–2011)". In: *Environmental health perspectives* 123.7, pp. 672–678.
McEvoy, Darryn, Iftekhar Ahmed, and Jane Mullett (2012). "The impact of the 2009 heat wave on Melbourne's critical infrastructure". In: *Local Environment* 17.8, pp. 783–796.
Meir, Talmor et al. (2013). "Forecasting the New York City urban heat island and sea breeze during extreme heat events". In: *Weather and Forecasting* 28.6, pp. 1460–1477.
Melecio-Vázquez, David et al. (2018). "Thermal Structure of a Coastal–Urban Boundary Layer". In: *Boundary-Layer Meteorology* 169 (1), pp. 151–161. ISSN: 15731472.
Miller, STK et al. (2003). "Sea breeze: Structure, forecasting, and impacts". In: *Reviews of geophysics* 41.3.
Miralles, Diego G et al. (2014). "Mega-heatwave temperatures due to combined soil desiccation and atmospheric heat accumulation". In: *Nature geoscience* 7.5, pp. 345–349.
National Weather Service, NOAA (May 2018). *National Weather Service New York, NY excessive heat page.* URL: https://www.weather.gov/okx/excessiveheat.
NOAA et al. (1998). *Automated Surface Observing System (ASOS) User's Guide.* URL: https://www.weather.gov/media/asos/aum-toc.pdf.
Pelliccioni, A et al. (2012). "Some characteristics of the urban boundary layer above Rome, Italy, and applicability of Monin–Obukhov similarity". In: *Environmental fluid mechanics* 12.5, pp. 405–428.
Peng, Roger D et al. (2011). "Toward a quantitative estimate of future heat wave mortality under global climate change". In: *Environmental health perspectives* 119.5, pp. 701–706.
Pullen, Julie et al. (2007). "Atmospheric response to local upwelling in the vicinity of New York–New Jersey harbor". In: *Journal of applied meteorology and climatology* 46.7, pp. 1031–1052.
Quan, Jiannong et al. (2013). "Evolution of planetary boundary layer under different weather conditions, and its impact on aerosol concentrations". In: *Particuology* 11.1, pp. 34–40.
Ramamurthy, P and E Bou-Zeid (2017). "Heatwaves and urban heat islands: a comparative analysis of multiple cities". In: *Journal of Geophysical Research: Atmospheres* 122.1, pp. 168–178.
Ramamurthy, Prathap and E Bou-Zeid (2014). "Contribution of impervious surfaces to urban evaporation". In: *Water Resources Research* 50.4, pp. 2889–2902.
Robinson, Peter J (2001). "On the definition of a heat wave". In: *Journal of Applied Meteorology and Climatology* 40.4, pp. 762–775.
Rose, Thomas et al. (2005). "A network suitable microwave radiometer for operational monitoring of the cloudy atmosphere". In: *Atmospheric research* 75.3, pp. 183–200.
Sánchez, JL et al. (2013). "A method to improve the accuracy of continuous measuring of vertical profiles of temperature and water vapor density by means of a ground-based microwave radiometer". In: *Atmospheric Research* 122, pp. 43–54.
Shrestha, Bhupal et al. (2021). "Overview and Applications of the New York State Mesonet Profiler Network". In: *Journal of Applied Meteorology and Climatology* 60.11, pp. 1591–1611.
Stéfanon, Marc et al. (2014). "Soil moisture-temperature feedbacks at meso-scale during summer heat waves over Western Europe". In: *Climate dynamics* 42.5, pp. 1309–1324.
Tewari, Mukul et al. (2019). "Interaction of urban heat islands and heat waves under current and future climate conditions and their mitigation using green and cool roofs in New York City and Phoenix, Arizona". In: *Environmental Research Letters* 14.3, p. 034002.
Thomas, Natalie P et al. (2020). "Mechanisms associated with daytime and nighttime heat waves over the contiguous united states". In: *Journal of Applied Meteorology and Climatology* 59.11, pp. 1865–1882.
Thompson, William T, Teddy Holt, and Julie Pullen (2007). "Investigation of a sea breeze front in an urban environment". In: *Quarterly Journal of the Royal Meteorological Society: A journal of the atmospheric sciences, applied meteorology and physical oceanography* 133.624, pp. 579–594.
Wang, Z et al. (2012). "Lidar measurement of planetary boundary layer height and comparison with microwave profiling radiometer observation". In: *Atmospheric Measurement Techniques* 5.8, pp. 1965–1972.
Wu, Yonghua et al. (2019). "Observation of heat wave effects on the urban air quality and PBL in New York City area". In: *Atmospheric Environment* 218, p. 117024.
Yu, Yunyue et al. (2008). "Developing algorithm for operational GOES-R land surface temperature product". In: *IEEE Transactions on Geoscience and Remote Sensing* 47.3, pp. 936–951.

Zhang, Yuanjie et al. (2020). "Aircraft observed diurnal variations of the planetary boundary layer under heat waves". In: *Atmospheric Research* 235, p. 104801.
Zhao, Lei et al. (2018). "Interactions between urban heat islands and heat waves". In: *Environmental research letters* 13.3, p. 034003.
Zuo, Jian et al. (2015). "Impacts of heat waves and corresponding measures: a review". In: *Journal of Cleaner Production* 92, pp. 1–12.

Appendix

$$p = p_0 \exp \frac{-gz}{RT_0}$$

$$\theta = T \left(\frac{p_0}{p} \right)^{\frac{R}{c_p}}$$

$$q = \frac{w}{1+w} = \frac{\frac{\varepsilon \rho_v' R_v T}{p-\rho_v' R_v T}}{1 + \frac{\varepsilon \rho_v' R_v T}{p-\rho_v' R_v T}}$$

$$Ri_b = \frac{g \Delta \bar{\theta}_v \Delta z}{\bar{\theta_v} \left[(\Delta \bar{U}^2) + (\Delta \bar{V}^2) \right]}$$

Table 2: Symbols and abbreviations used in the paper.

Symbol/Abbreviation	Definition
σ	Standard deviation
θ	Potential temperature
q	Specific humidity
U	Horizontal wind speed
w	Vertical velocity
UBL	Urban boundary layer
MLH	Mixed layer height

Figures

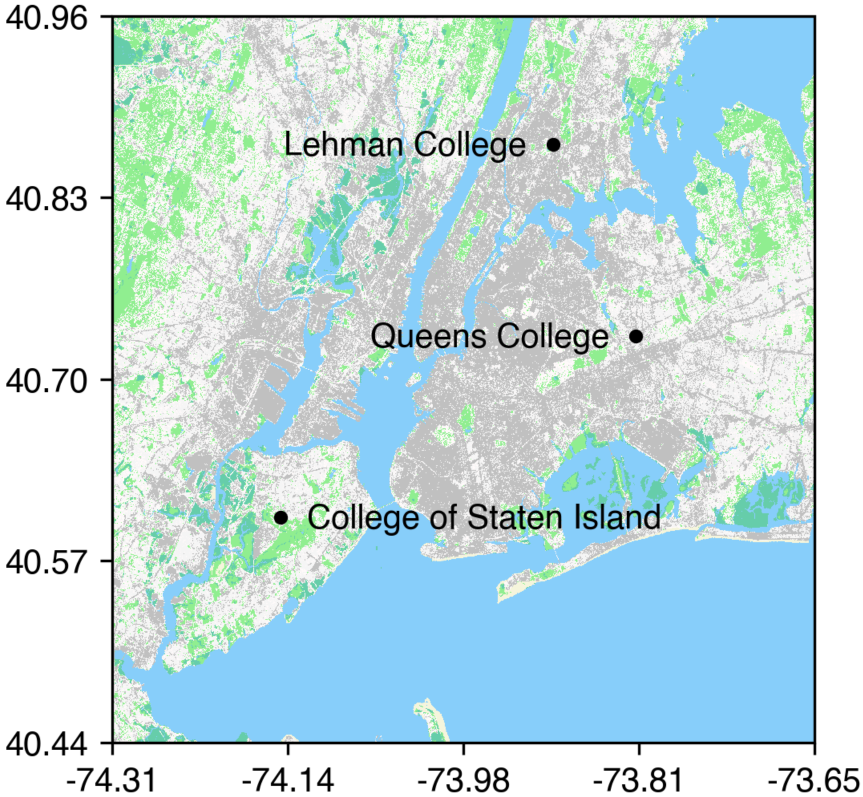

Figure 1: Observation sites overlaid on NLCD land cover types..

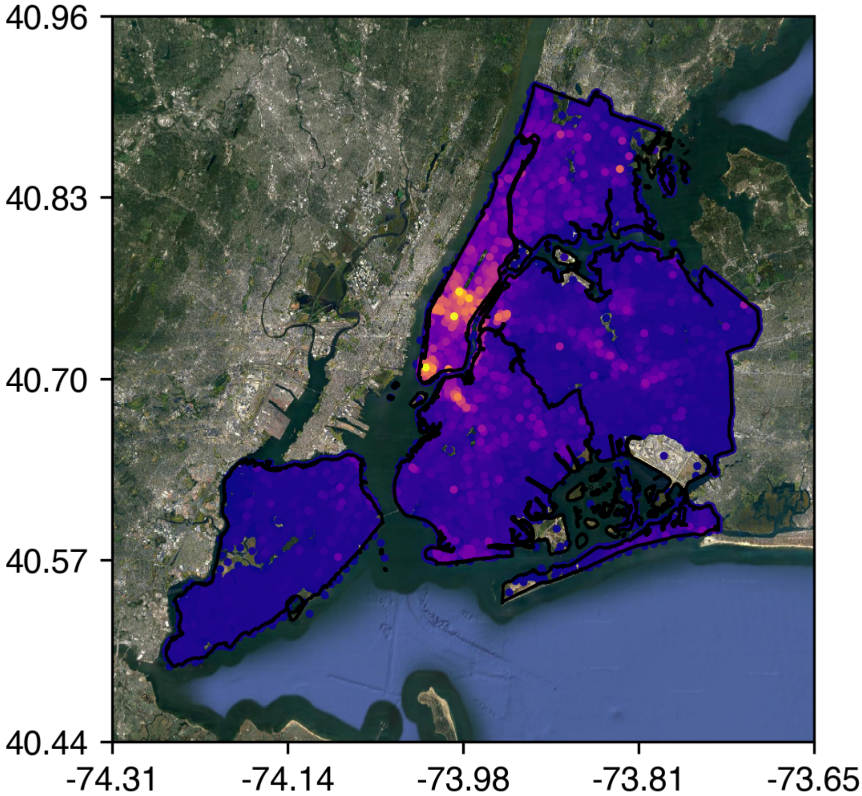

Figure 2: Building heights in New York City. Taken from NYC DOB data.

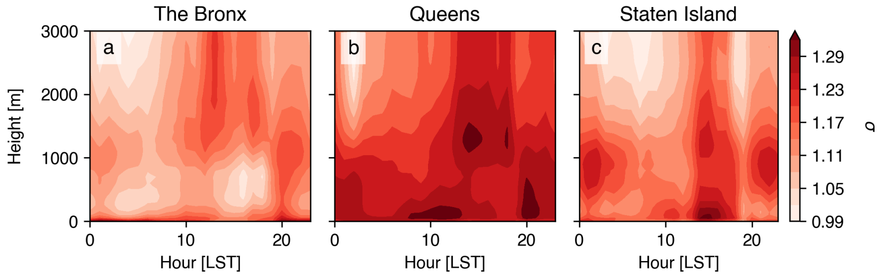

Figure 3: Anomalies of θ during extreme heat events relative to the climatology over the urban boundary layer.

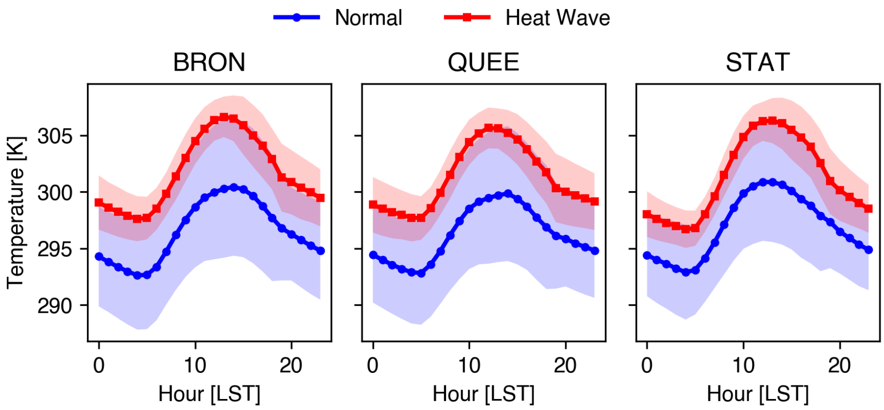

Figure 4: Anomalies of temperature during extreme heat events relative to the climatology at the surface.

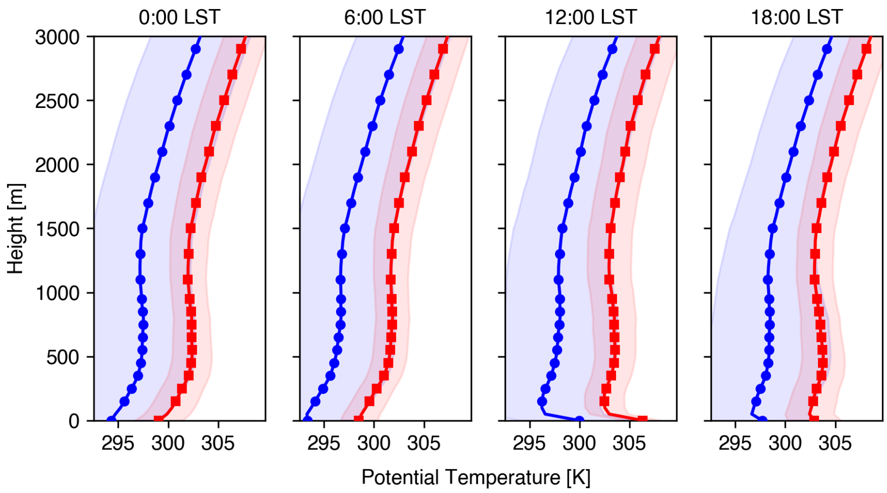

Figure 5: Vertical profiles of θ in the Bronx during normal days (blue) and extreme heat events (red).

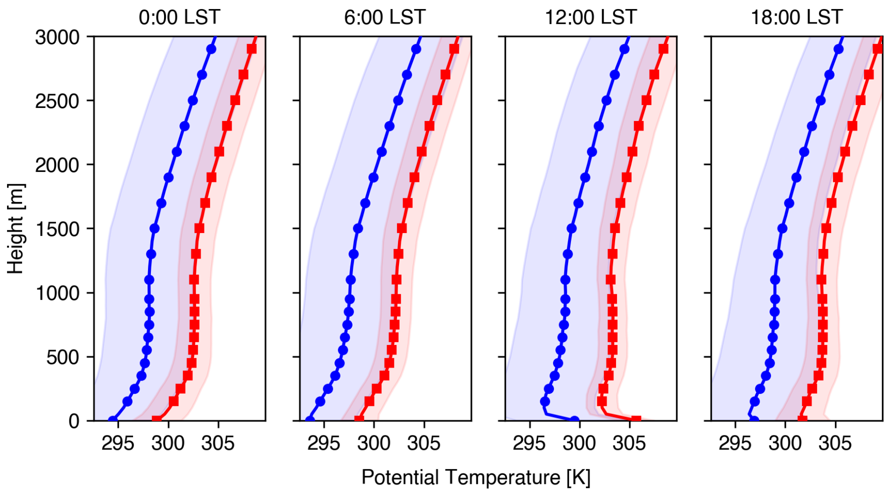

Figure 6: Vertical profiles of θ in Queens during normal days (blue) and extreme heat events (red).

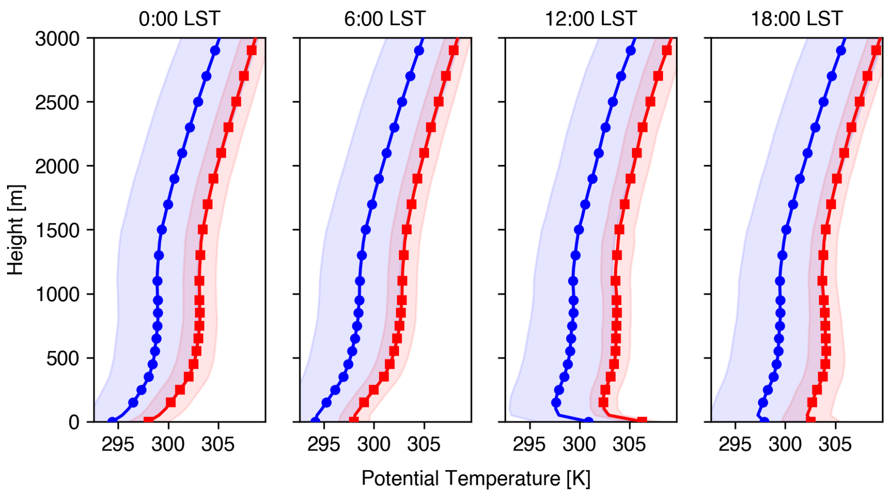

Figure 7: Vertical profiles of θ in Staten Island during normal days (blue) and extreme heat events (red).

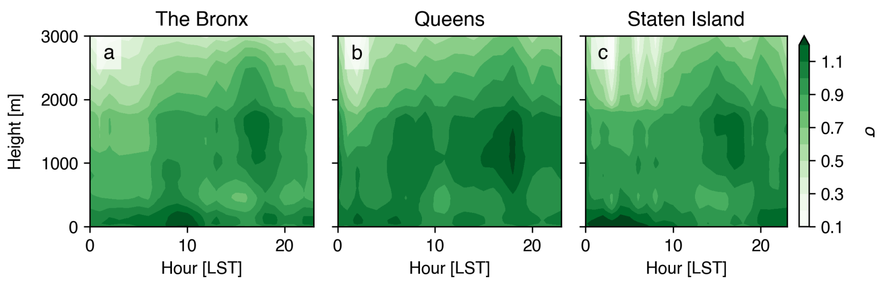

Figure 8: Anomalies of q during extreme heat events relative to the climatology over the urban boundary layer.

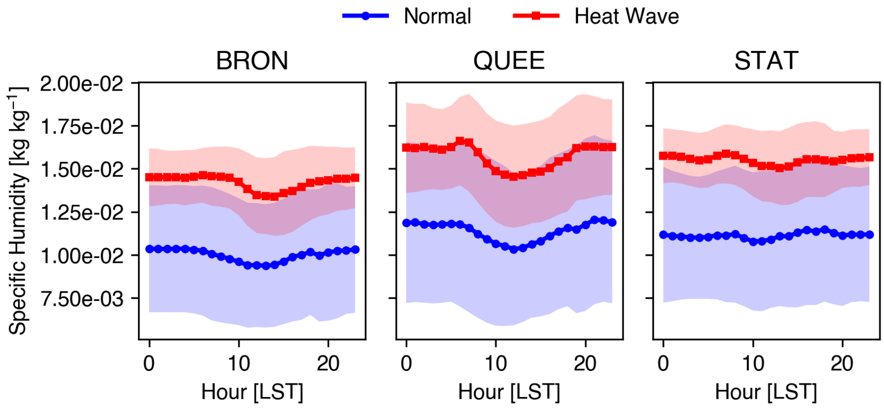

Figure 9: Anomalies of q during extreme heat events relative to the climatology at the surface.

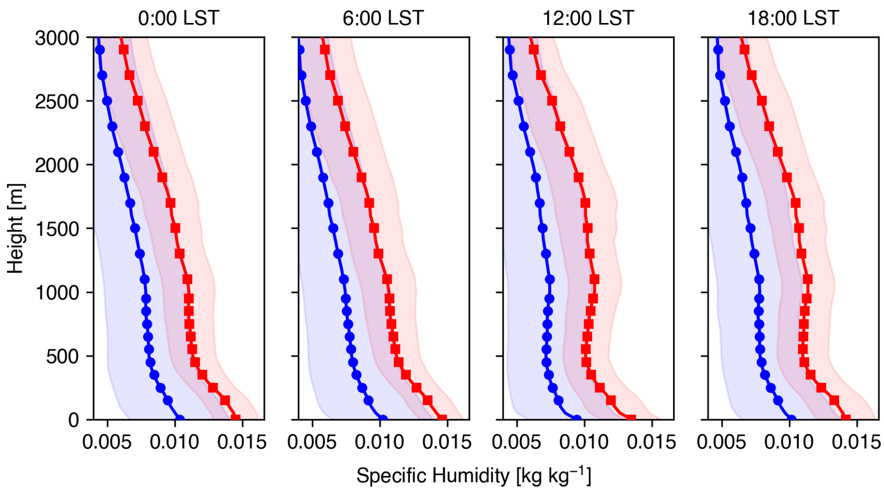

Figure 10: Vertical profiles of q in the Bronx during normal days (blue) and extreme heat events (red).

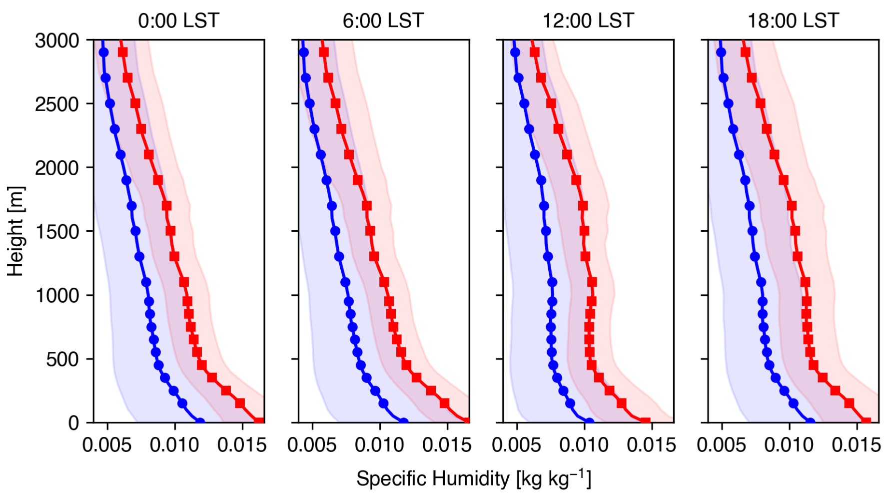

Figure 11: Vertical profiles of q in Queens during normal days (blue) and extreme heat events (red).

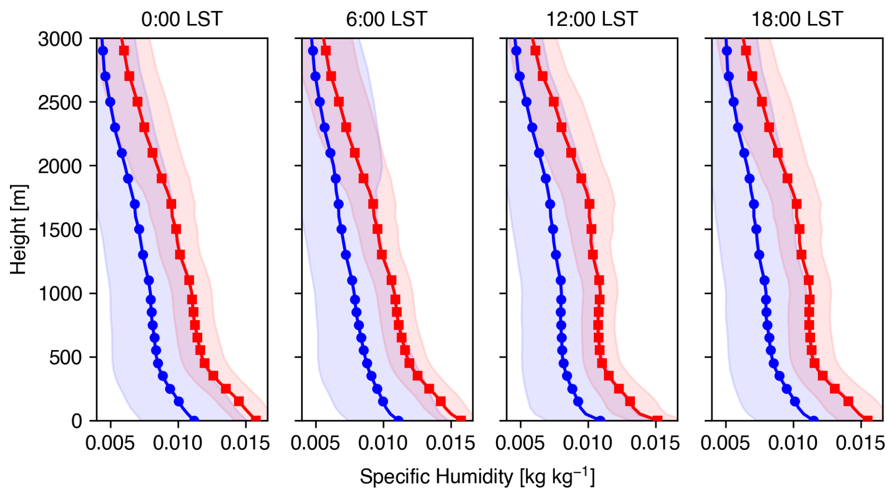

Figure 12: Vertical profiles of q in Staten Island during normal days (blue) and extreme heat events (red).

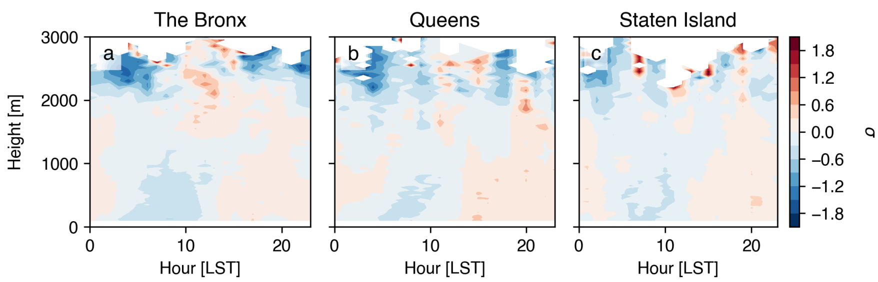

Figure 13: Anomalies of U during extreme heat events relative to the climatology over the urban boundary layer.

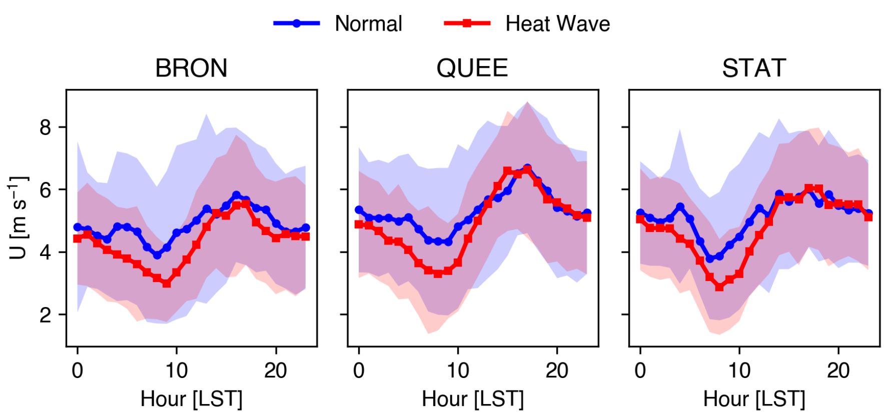

Figure 14: Anomalies of low-level U during extreme heat events relative to the climatology.

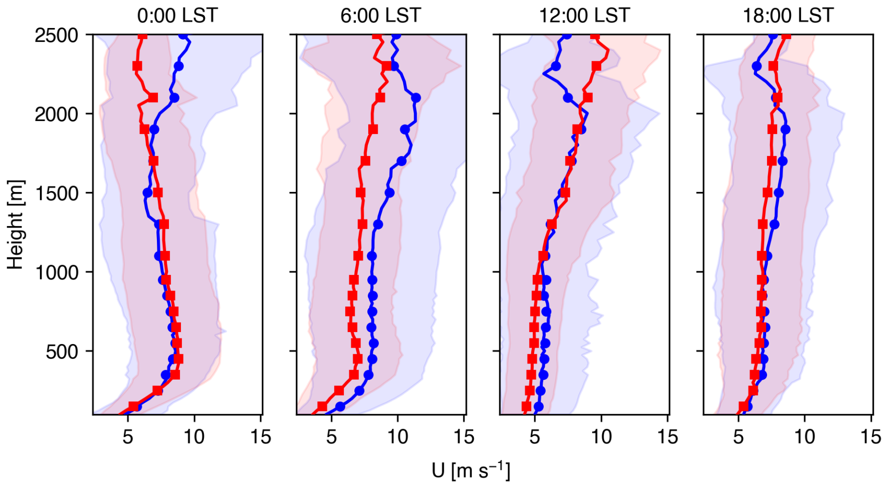

Figure 15: Vertical profiles of U in the Bronx during normal days (blue) and extreme heat events (red).

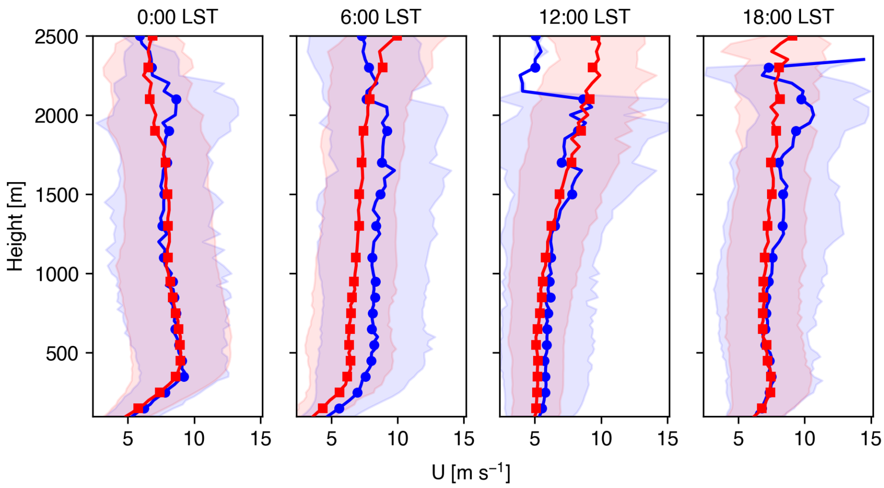

Figure 16: Vertical profiles of U in Queens during normal days (blue) and extreme heat events (red).

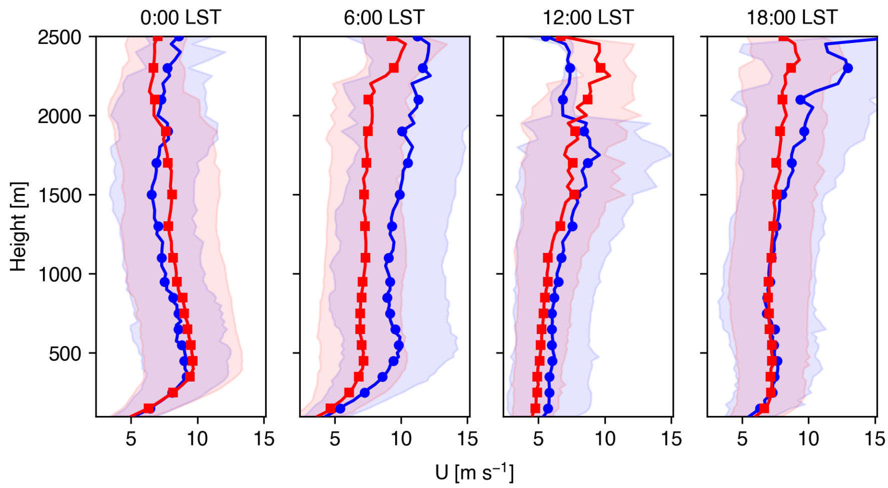

Figure 17: Vertical profiles of U in Staten Island during normal days (blue) and extreme heat events (red).

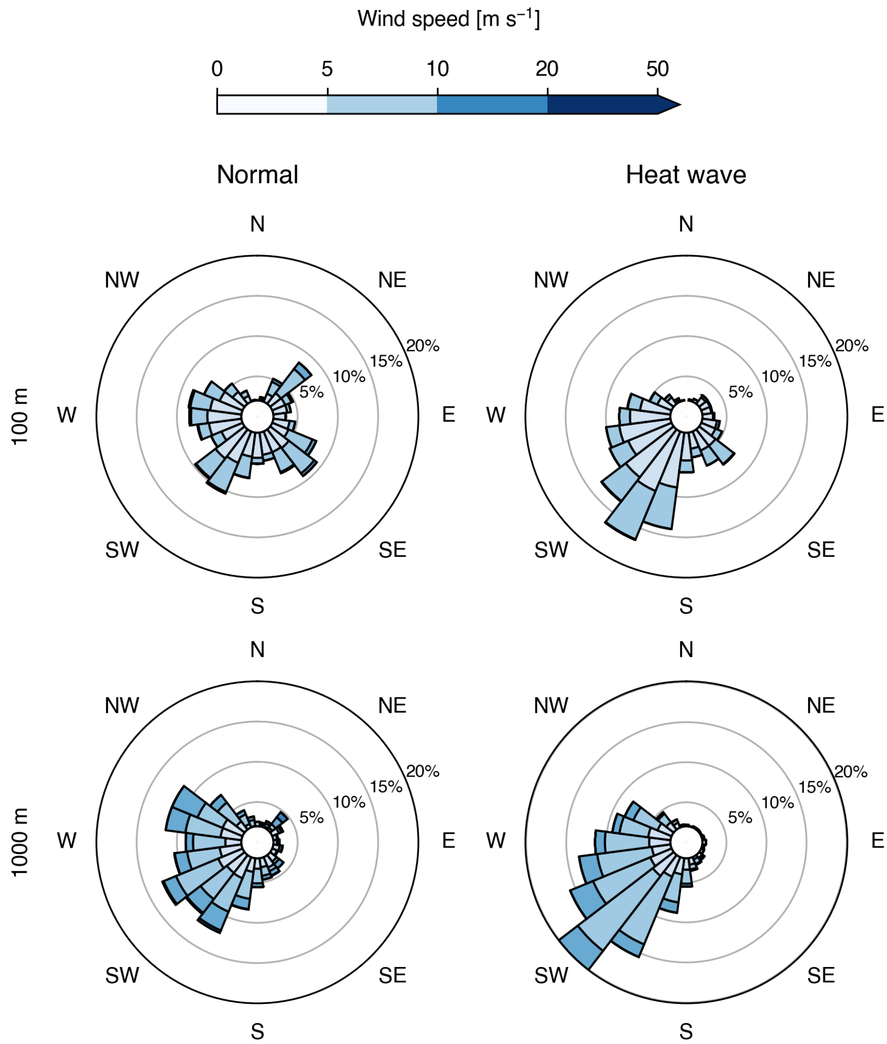

Figure 18: Horizontal winds in the lower-level (100 m) and mid-level of the urban boundary layer over the Bronx.

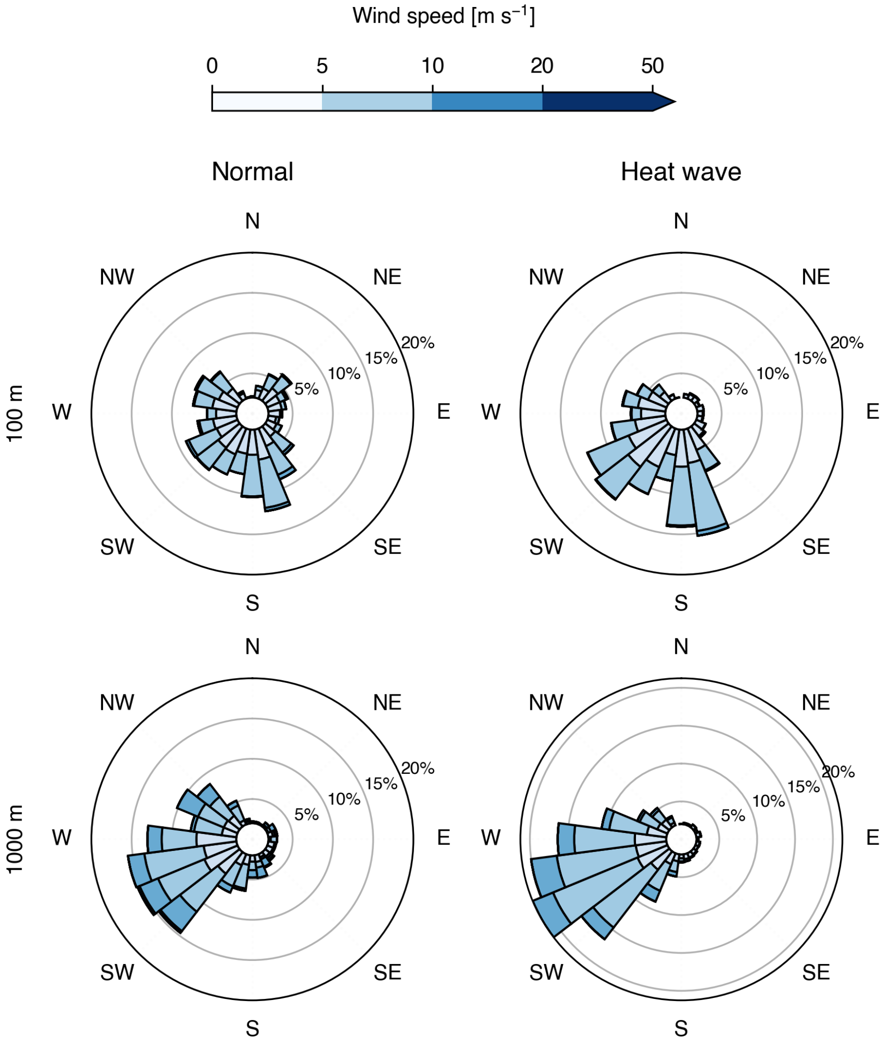

Figure 19: Horizontal winds in the lower-level (100 m) and mid-level of the urban boundary layer over Queens.

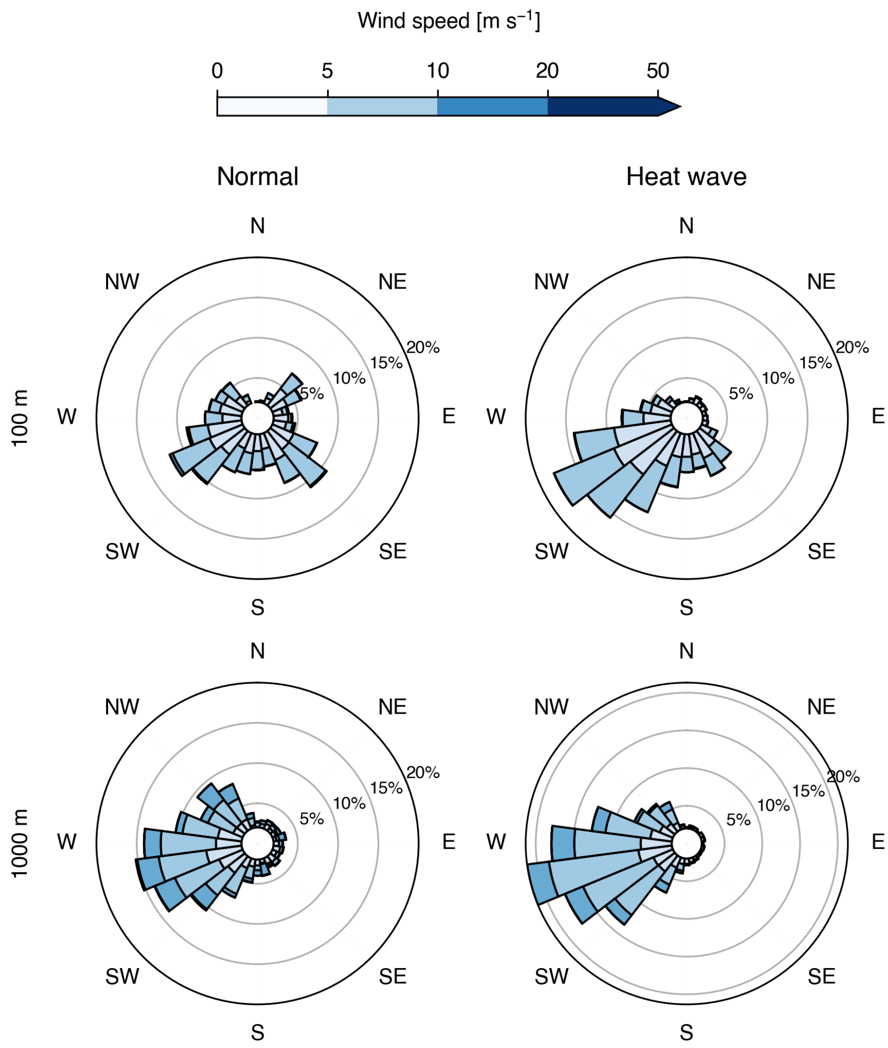

Figure 20: Horizontal winds in the lower-level (100 m) and mid-level of the urban boundary layer over Staten Island.

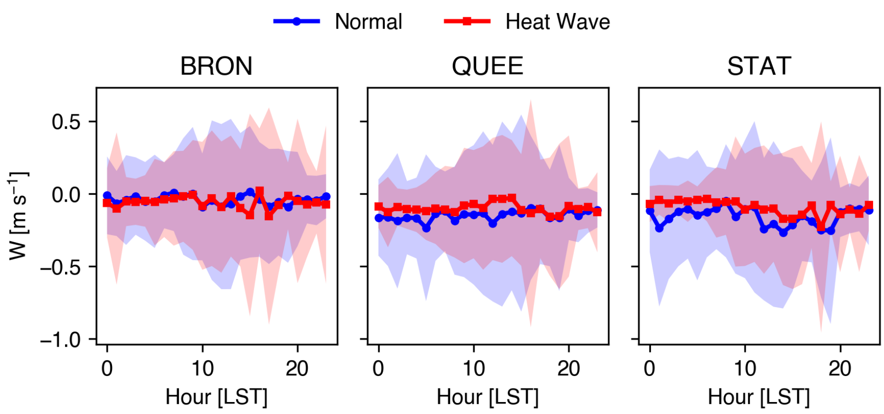

Figure 21: Anomalies of low-level w during extreme heat events relative to the climatology.

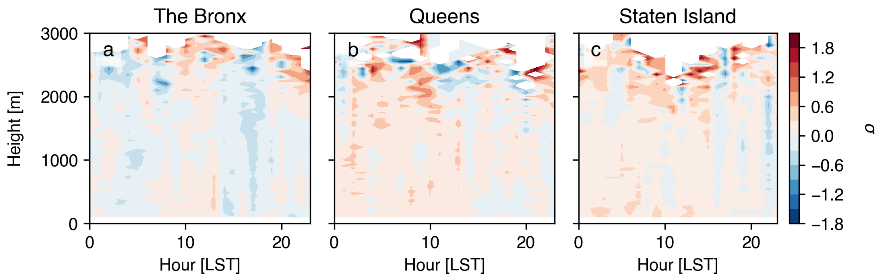

Figure 22: Anomalies of w during extreme heat events relative to the climatology over the urban boundary layer.

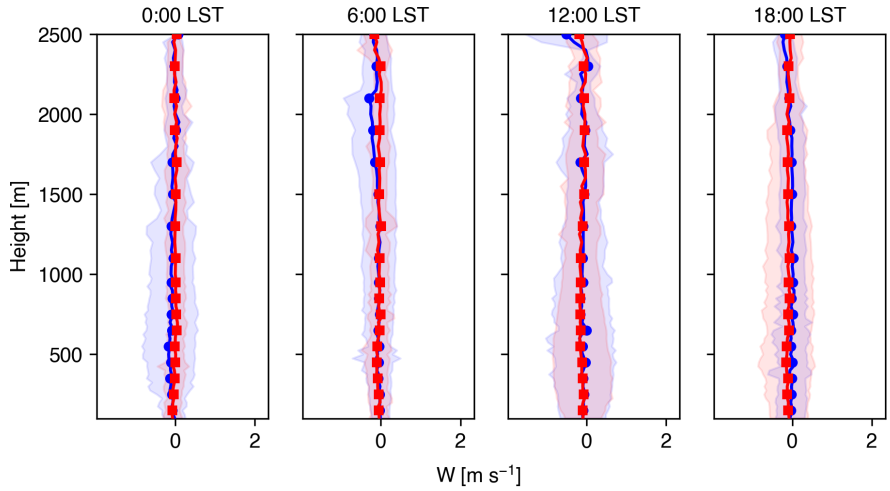

Figure 23: Vertical profiles of w in the Bronx during normal days (blue) and extreme heat events (red).

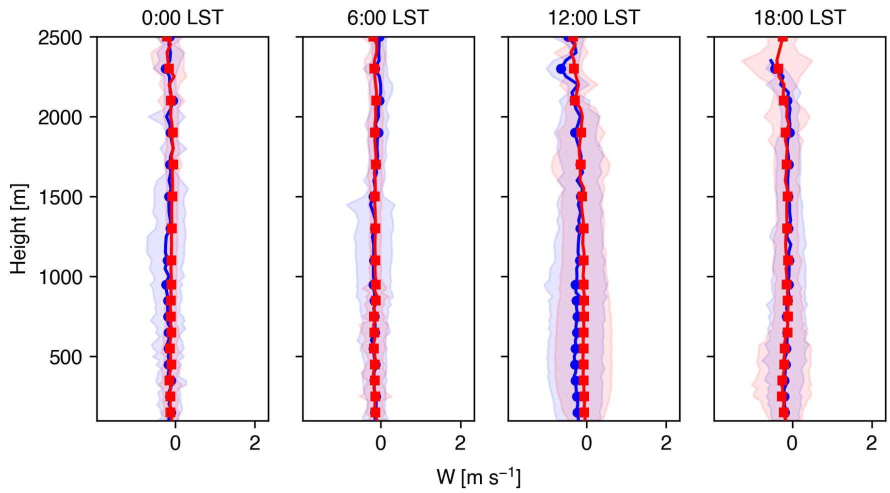

Figure 24: Vertical profiles of w in Queens during normal days (blue) and extreme heat events (red).

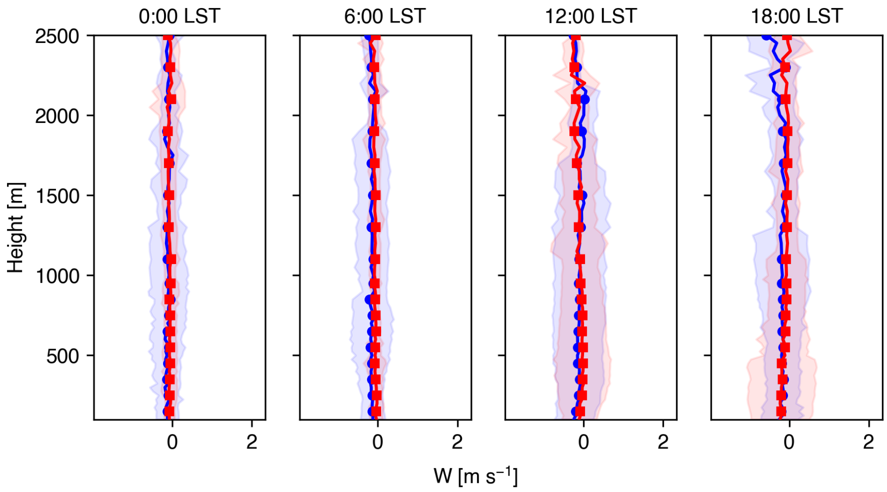

Figure 25: Vertical profiles of U in Staten Island during normal days (blue) and extreme heat events (red).

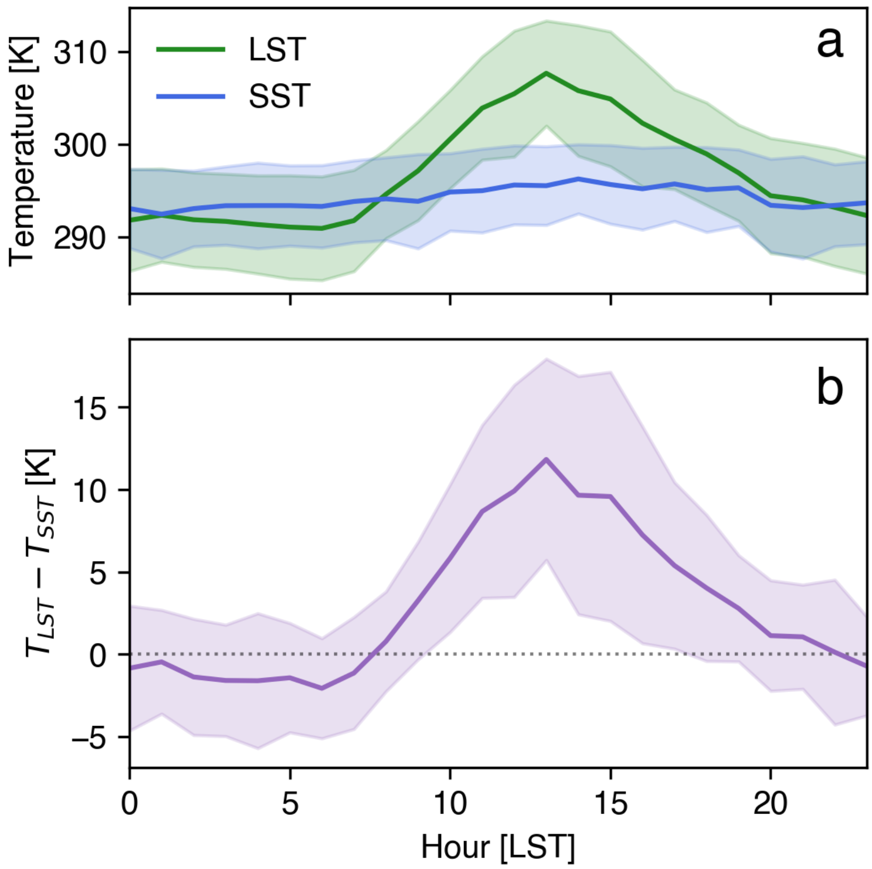

Figure 26: Temperature difference between Queens and New York Bight.

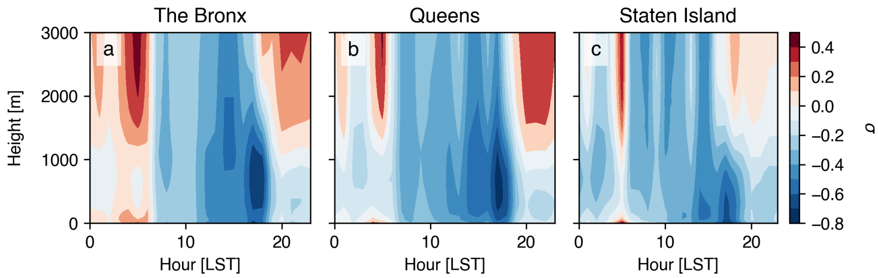

Figure 27: Anomalies of θ for normal days with a sea breeze relative to normal days without a sea breeze.

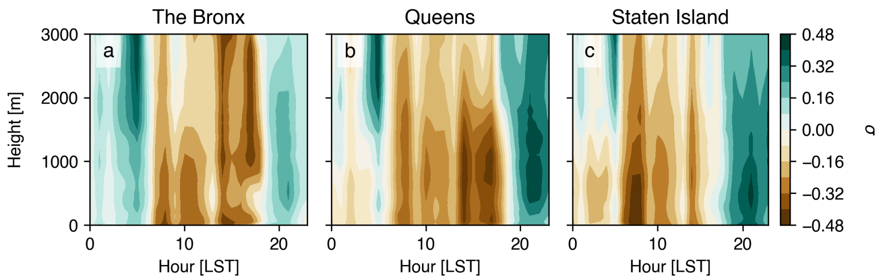

Figure 28: Anomalies of q for normal days with a sea breeze relative to normal days without a sea breeze.

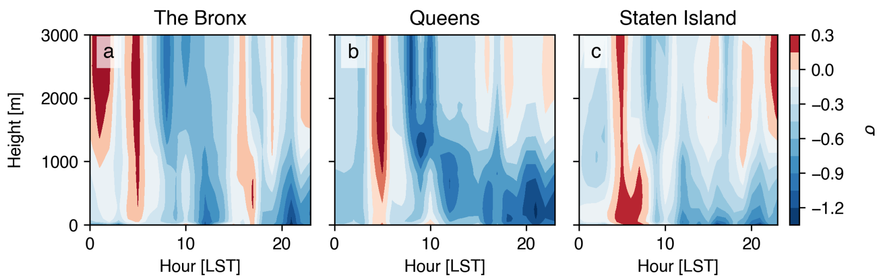

Figure 29: Anomalies of θ for heat wave days with a sea breeze relative to heat wave days without a sea breeze.

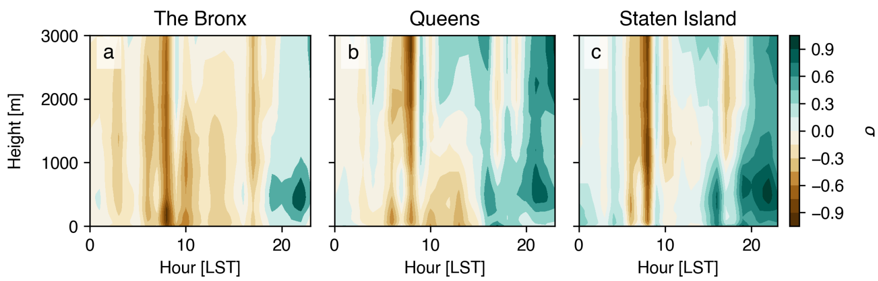

Figure 30: Anomalies of q for heat wave days with a sea breeze relative to heat wave days without a sea breeze.

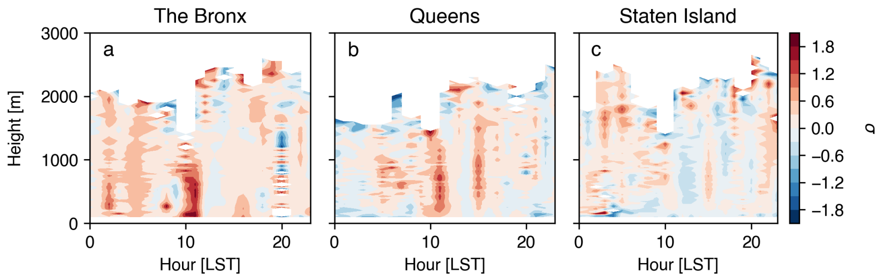

Figure 31: Anomalies of w for heat wave days with a sea breeze relative to heat wave days without a sea breeze.

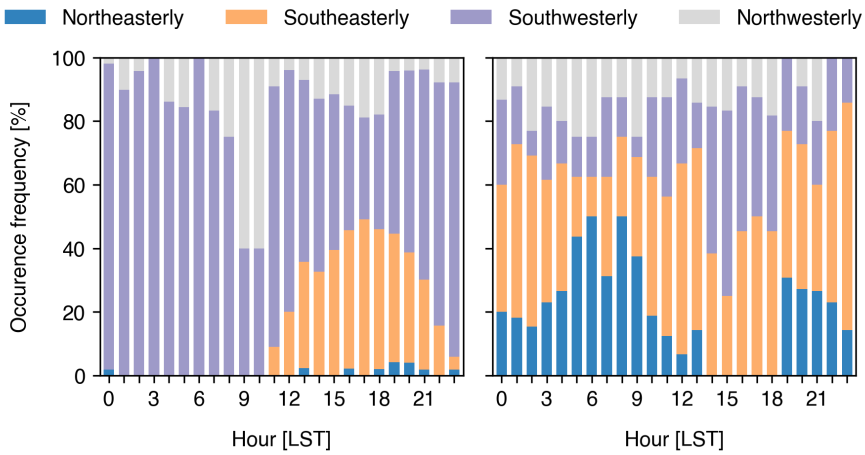

Figure 32: Occurrence frequency of wind directions at 100 m in the Bronx.

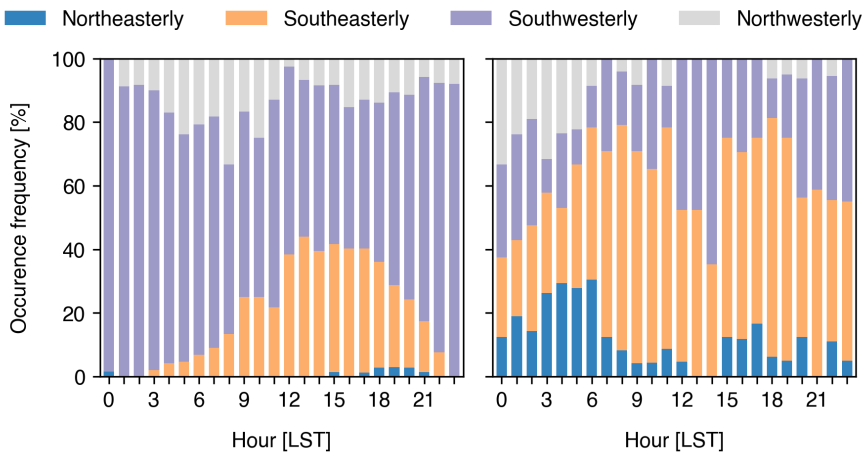

Figure 33: Occurrence frequency of wind directions at 100 m in Queens.

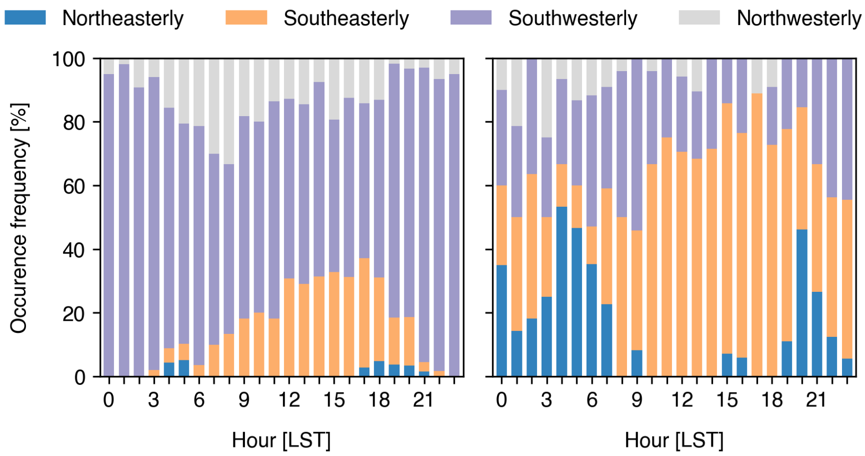

Figure 34: Occurrence frequency of wind directions at 100 m in Staten Island.